Volume 3
Number 3
March 2023
Pages 437–630

# Environmental Science
## Atmospheres

rsc.li/esatmospheres

ISSN 2634-3606

ROYAL SOCIETY OF CHEMISTRY

**PAPER**
Joseph P. Hupy, Patricia A. Cleary *et al.*
Observations of coastal dynamics during lake breeze at a shoreline impacted by high ozone

Environmental Science: Atmospheres

ROYAL SOCIETY OF CHEMISTRY

PAPER

View Article Online
View Journal | View Issue



Cite this: *Environ. Sci.: Atmos.*, 2023, **3**, 494

# Observations of coastal dynamics during lake breeze at a shoreline impacted by high ozone†

Joseph Tirado,[a] Akagaonye O. Torti,[a] Brian J. Butterworth,[bc] Kevin Wangen,[a] Aidan Voon,[a] Benjamin Kies,[a] Joseph P. Hupy,*[d] Gijs de Boer,[bce] R. Bradley Pierce,[fg] Timothy J. Wagner[f] and Patricia A. Cleary *[a]

The lake breeze circulation along Lake Michigan is associated with high tropospheric ozone concentrations at shoreline locations. The 2021 Wisconsin's Dynamic Influence of Shoreline Circulation on Ozone (WiscoDISCO-21) campaign involved atmospheric measurements over Chiwaukee Prairie State Natural Area in Southeastern Wisconsin from May 21–26, 2021. Three different platforms, two uncrewed aerial systems (UAS) and a Doppler lidar instrument, were used to collect data on this campaign, supplemented by a ground-based Wisconsin DNR maintained regulatory monitor at the site. A Purdue University M210 multirotor copter, and the University of Colorado RAAVEN fixed-wing aircraft were flown in coordination. Using data from the ground station, RAAVEN and onsite lidar, lake breezes were detected on several days of the campaign. The longest sustained lake breezes during the campaign were detected on May 22, 2021, from 17:00–21:38 UTC and on May 24, 2021, from 14:24–22:51 UTC. The presence of the lake breezes correlated with detected temperature inversions measured from the RAAVEN and high ozone events measured from the M210. Lake breezes were investigated with their relationship to vertical profiles measured on the UAS, ozone concentrations, and marine boundary layer height observed with Doppler lidar to demonstrate a multi-layered lower atmosphere. A buoyant internal boundary layer was observed over land from 40–100 m AGL below highest ozone concentrations. Marine layer extent was investigated through minimum buoyancy and Richardson number analysis, showing limited vertical mixing at altitudes up to 200 m AGL, below easterly lake breeze circulation patterns extending upward to 400 m AGL in the late day.

Received 10th August 2022
Accepted 29th December 2022

DOI: 10.1039/d2ea00101b

rsc.li/esatmospheres



## Environmental significance

Tirado, *et al.* observations of coastal dynamics during lake breeze at a shoreline impacted by high ozone communities surrounding Lake Michigan are impacted by high ozone, which is influenced by the meteorology of lake breeze. Improvements to the understanding of the atmosphere in a transitional coastal environment can allow for improved modeling of poor air quality events in the region. The use of uncrewed aerial systems and Doppler lidar have demonstrated a complex layering of the atmosphere with high ozone concentrations at low altitudes (40–100 m AGL) during lake breeze above a mixed internal boundary layer over land. Lake breeze easterly circulation patterns were shown to extend up to 450 m AGL. The investigations of the lower atmosphere by connecting domains between instruments can inform resolution and parameterization improvements to meteorological and air quality models.

## 1. Introduction

The 2021 Wisconsin's Dynamic Influence of Shoreline Circulation on Ozone (WiscoDISCO-21) campaign was designed to measure the characteristics of lake breezes at the Lake Michigan shoreline, and their impact on high ozone events above Chiwaukee Prairie, Wisconsin. Ozone forms in the lower troposphere, primarily from anthropogenic emissions when nitrogen oxides produced by burning fossil fuels and volatile organic compounds (VOC) react in the atmosphere in the presence of sunlight. Tropospheric ozone causes many harmful effects to humans and the environment. Studies on ozone's effects on vegetation have demonstrated that exposure to high levels of ozone can result in lower crop yields and increased

[a]*Department of Chemistry and Biochemistry, University of Wisconsin-Eau Claire, USA. E-mail: clearypa@uwec.edu*

[b]*Cooperative Institute for Research in Environmental Sciences, University of Colorado Boulder, Boulder, CO, USA*

[c]*Physical Sciences Laboratory, National Oceanic and Atmospheric Administration, Boulder, CO, USA*

[d]*School of Aviation and Transportation Technology, Purdue Polytechnic, Purdue University, West Lafayette, IN, USA*

[e]*Integrated Remote and* In Situ *Sensing, University of Colorado Boulder, Boulder, CO, USA*

[f]*Space Science and Engineering Center, University of Wisconsin–Madison, USA*

[g]*Atmospheric and Oceanic Sciences, University of Wisconsin–Madison, USA*

† Electronic supplementary information (ESI) available. See DOI: https://doi.org/10.1039/d2ea00101b

damage to vegetation.[1] Studies have also shown that tropospheric ozone can decrease lung functions in humans and animals.[2–4]

Because of such negative impacts, it is important to understand why ozone concentrations have historically exceeded federal ozone standards in parts of Wisconsin that border Lake Michigan. High ozone events occurring in this coastal zone have been attributed to lake breeze circulations from Lake Michigan.[5–12] During the summer, the stable marine layer can trap and transport air near the Lake Michigan surface, with lake breeze events working to advect this marine layer air toward and over the shoreline.

Atmospheric temperature inversions increase tropospheric ozone formation by trapping nitrogen oxides and VOCs in the atmosphere, allowing them to react in a concentrated area. When the general circulation advects air from the south, urban emissions from the Chicago, Illinois and Gary, Indiana region are pushed out over the lake, where the stable marine layer provides an optimal environment for chemical reactions that work to form ozone.[11–13] This process has been demonstrated to be particularly active if land breezes develop overnight which enhance transport of anthropogenic emissions from these urban centers over the water where it becomes trapped in the marine layer.[11] This leads to a confined air mass capable of ozone production in the atmosphere above a body of water which can be advected back on land during lake breezes.[5,10,12] There is a clear relationship between lake breeze and high ozone events at the ground level.[5,6,10,11] Firstly, many studies have observed the transportation of ozone and other pollutants from over Lake Michigan[6,10,11,14] as well as from over other great lakes[15–17] due to lake breeze events in the spring and summer. Furthermore, a past study at a Lake Michigan site has found that land breezes during the summer have been responsible for transporting anthropogenic emissions from over land to over Lake Michigan.[11] A 2009 study has also observed that the marine layer near the Great Salt Lake can result in the mixing of anthropogenic emissions and can result in the formation of high ozone concentrations.[18]

The impact of turbulent mixing of air on ozone within and above a shoreline marine inversion has been investigated often in connection with lake and sea breeze circulations, but with limited vertical profile studies. High ozone concentrations observed in Houston were associated with the sea breeze circulation resulting from the Gulf of Mexico and Galveston Bay shorelines.[19] Similarly, vertical profiling of sea and lake breeze circulations along coastal Nova Scotia and above a Saskatchewan Lake showed limited mixing with high ozone above a thermal internal boundary layer (IBL).[20,21] During the Border Air Quality and Meteorology Study (BAQS-Met) on the southern Great Lakes, research aircraft flights observed high concentrations of ozone aloft[16] without many connections between high over-water ozone concentrations observed *via* ship and the higher altitude flights of aircraft. During the 2017 Lake Michigan Ozone Study (LMOS), research aircraft were flown to 30 m above lake level where they observed the highest concentrations of offshore ozone along Lake Michigan.[5,12] Over water ozone models were shown to have a high bias relative to ferry observations on Lake Michigan[22] and resolving the vertical structure and mixing, along with improved emissions profiles, appear to be key in improving model fidelity.[23–25] Development of models for vertical structure of over water marine layer stratification and development of internal boundary layers is of key interest for lake-effect snow forecasting and pollutant dispersion modelling.[26]

Recent studies have shown that the use of Uncrewed Aerial Systems (UAS) in studying vertical profiles in the atmosphere can be highly effective.[27–30] UAS have been used effectively in the past to measure boundary layer ozone concentrations.[28] During the OWLETs campaign UAS were used to measure over water ozone concentrations.[31] A study in New Zealand found that using UAS to measure atmospheric conditions such as temperature and humidity in a coastal region was also highly successful.[29] Furthermore, the use of UAS has been used in the past to successfully measure chemical concentrations, pollutant transportations and the night-time boundary level height.[30]

During WiscoDISCO-21, UAS were used to measure the vertical variability in ozone concentrations, as well as the thermodynamic and kinematic gradients existing across the lake breeze front and coastal boundary. These data have been used to derive information on boundary layer heights above both near-coastal Lake Michigan and the Chiwaukee Prairie to help understand how the marine layer plays a role in ozone transport during a lake breeze. The overlapping domains of each platform allowed for a more complete coverage for the lower atmosphere to elucidate the complex layering of the atmosphere and the impact that has on ozone abundance during high ozone events. Such data can be useful to aid in parameterizations of ozone transport in a coastal environment. During the 2017 Lake Michigan Ozone Study, manned aircraft over water flights observed high ozone within the lowest 100 m above lake level,[5,12] which is a domain more safely sampled by UAS for a longer duration. As with any intensive atmospheric sampling experiment, this field campaign provided extended information on the atmosphere for a limited amount of time in May 2021 and must be understood to incorporate a framework for interpretation of such data, but is not extensive to all atmospheric conditions over a broader range of time. However, flying UAS into low altitude space of inversion allows for a targeted exploration of the lower atmosphere in a dynamic coastal environment, capable of measuring both meteorological and chemical components of the atmosphere. This allows for a more thorough representation of the atmosphere than one remote sensing device alone and with more coverage of the lower atmosphere than lidar, manned aircraft, or sondes which do not make near-surface observations for any long duration.

## 2. Experimental

The WiscoDISCO-21 study took place in southeastern Wisconsin (USA), at Chiwaukee Prairie State Natural Area in Kenosha County (see Fig. 1). The Chiwaukee Prairie State Natural Area is 485 acres and is managed by the Wisconsin Department of Natural Resources (DNR), bordering the Lake Michigan shoreline. An air quality monitoring station is maintained at

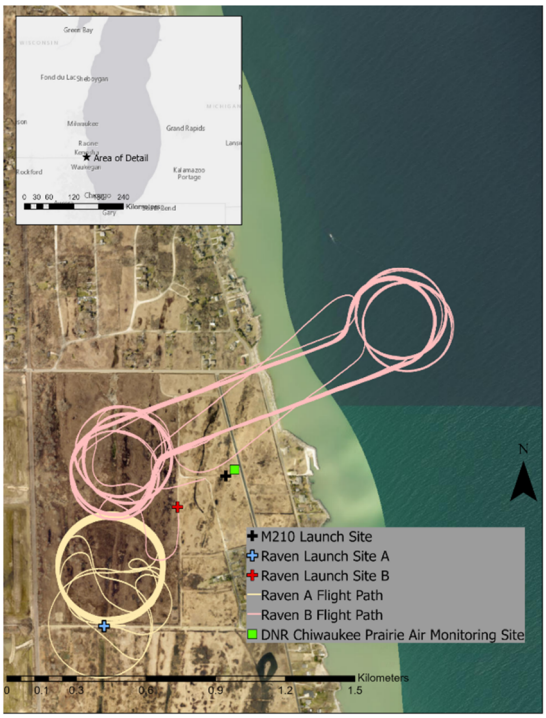


Fig. 1 Research site map: displaying the launch locations of the M210, and RAAVEN for over land flights A (flight path in yellow) and partial over water flights B (flight path in pink).

Chiwaukee Prairie (AIRS ID: 55-059-0019) by the Wi-DNR. The shelter for this monitoring station additionally housed a Doppler lidar during the summer of 2021. Intensive sampling of UAS flights lasted six days from May 21, 2021, to May 26, 2021. In addition to the surface instrumentation, two UAS platforms were deployed to capture information on the vertical structure of the lower atmosphere. A detailed description of the platforms, flight plans and measurement strategies used during WiscoDISCO-21 is provided in Cleary, *et al.*[32] All data are available through a WisocDISCO-21 community data repository.[33]

Data collection *via* UAS occurred on May 21, 22, 24, 25, and 26, 2021 from 13:00 to 22:00 UTC. The DJI M210 quadcopter was operated between the surface and 120 meters above ground level (m AGL), up to six times a day for about 15 minutes per flight (see Fig. 1). The M210 operated with battery power with no exhaust emissions. Data acquisition for each M210 flight was from a single slow vertical ascent from a fixed launch point. The M210 was equipped with a 2B Technologies Personal Ozone Monitor (POM) which measured $O_3$ using UV absorption with an in-series active subtraction for water vapor interference at a 10 s duty cycle. The POM measured ozone concentrations in parts per billion (ppb) at a frequency of 0.1 Hz. POM performance has been shown to be affected by large temperature variations in a vertical profile,[34] however here we use the ozone data semi-quantitatively over a smaller temperature gradient.

An Interment Systems iMET-XQ2 meteorology sensor (iMET) with GPS satellite capability mounted to the M210 measured temperature, relative humidity, and pressure at a frequency of 1 Hz (see Table 1).

The M210 flight log recorded GPS positioning and flight at 100 Hz. To align the three different logging systems to one standard time, a time stamp for 90 s averaged data from all instrumentation on the M210 was generated by using the M210 time stamp as primary and adjusting to a time offset in either the POM or the iMET for the start of a flight, then averaged each variable for every 90 seconds interval of the flight. A $1\sigma$ is presented as the uncertainty for the 90 s averages. Overall, the M210 completed 24 flights over the course of the campaign.

The RAAVEN fixed-wing UAS flew up to 500 m AGL, up to three times per day for approximately 2 hours per flight with battery power and no exhaust emissions. RAAVEN flights covered two separate flight patterns, including one that focused on sampling the vertical structure over land (A) and a second that included sampling over both water and land (B), including vertical profiles in both locations and spatial sampling of variability at a variety of altitudes (Fig. 1). On May 21 and 22 the RAAVEN flew only over land in pattern A. On May 24, 25, and 26 the RAAVEN followed flight path B, taking it over Lake Michigan for approximately half of the flight. The RAAVEN was equipped with a payload suite to measure thermodynamic and kinematic conditions in the lower atmosphere. This included a multi-hole pressure probe (MHP) from Black Swift Technologies, a pair of 174 RSS421 PTH (pressure, temperature, humidity) sensors from Vaisala, Inc., a pair of Melexis MLX90614 IR 176 thermometers, and a VectorNav VN-300 inertial navigation system (INS) (see Table 1). In total, the RAAVEN completed 12 flights over the course of the campaign. Intercomparison between UAS platforms and the air quality ground station observations showed good agreement (Fig. S8 and S9 in ESI†).

Finally, a Doppler lidar was deployed for WiscoDISCO-21 (Halo Photonics Stream Line XR Doppler lidar)[35] on the roof of the Chiwaukee Prairie air monitoring station. The Doppler lidar utilized pulses of near-infrared radiation at a wavelength of 1.5 μm. Doppler lidar observations measured backscatter intensities, wind speeds and directions (see Table 1). The wind profiles were derived from six-point velocity azimuth display (VAD) scans. The depth of the retrieved wind profiles varied

Table 1 Measurements by each platform during WiscoDISCO-21: ozone ($O_3$), temperature ($T$), pressure ($P$), relative humidity (% RH), zonal wind velocity ($u$), meridional velocity ($v$) and other parameters

| Platform | $O_3$ (ppb) | $T$ (°C) | $P$ (kPa) | RH (%) | $u$ (m s$^{-1}$) | $v$ (m s$^{-1}$) | Other |
|---|---|---|---|---|---|---|---|
| M210 | x | x | x | x | | | |
| RAAVEN | | x | x | x | x | x | Sky brightness, surface brightness |
| Doppler lidar | | | | | x | x | Backscatter intensity, wind vertical velocity |

significantly from as shallow as 100 m AGL to as deep as 2 km AGL as the lidar depends on the presence of scatterers in order to have a detectable signal return.

# 3. Results and discussion

## 3.1 Synoptic meteorology

During the week of May 21–26, 2021 the synoptic meteorological conditions had some element of southerly wind flow due to the passage of a high pressure system near the Ohio Valley which lends itself to anti-cyclonic circulations in the Lake Michigan region.[6,36,37] On May 21–22 synoptic winds in the general region were southerly moving to southwesterly. On May 23 a low pressure system front moved through northern Lake Michigan turning winds to northeasterly. On May 24 the move of the low pressure trough to the east made winds shift from easterly to southerly through the day. By May 25, the high pressure system around the Ohio River Valley moved southward to the gulf coast and winds were westerly/southwesterly for most of the day. A front moved in on May 26, 2021 making winds northerly.

## 3.2 Lake breeze onset and corresponding ground observations

The presence of a lake breeze or marine air incursion over the Chiwaukee Prairie was identified using meteorological data collected at 4.5 m AGL at the ground air monitoring station in Chiwaukee Prairie from 21–26 May 2021. Lake breeze onset was defined as sustained shifts in wind direction from >180° to <180° & >90°, with corresponding lower wind speeds and a drop in temperature assuming no other frontal activity was observed in the region. This last criterion excludes sampling conducted on May 23, 2021, as a synoptic cold front traversed the region on this date (Fig. 2).

The characteristic sawtooth structure in wind direction on May 21 shows the development and advancement of a lake breeze circulation 3 times on that day. Seven distinct lake breeze onset events were identified (in grey, Fig. 2) where marine air influence was mostly southeasterly or easterly were highlighted. On May 25, a lake breeze was established for only a short time in the early morning after which high westerly winds prevented onshore flow for the rest of the day. When looking at key chemical measurements from the site, the lake breeze occurrences tended to correspond with the highest ozone concentrations. The anti-correlation between $NO_x$ and $O_3$ is apparent in the NO, $NO_2$ and $NO_y$ observations at the site and $NO_y$ is made up of mostly NO + $NO_2$ at the site, indicating local emissions (Fig. 3).

Lake breeze onset was identified to highlight relationships between lake breeze onset and temperature, wind speed and ozone concentrations (Fig. 2a–c). Air temperature reliably

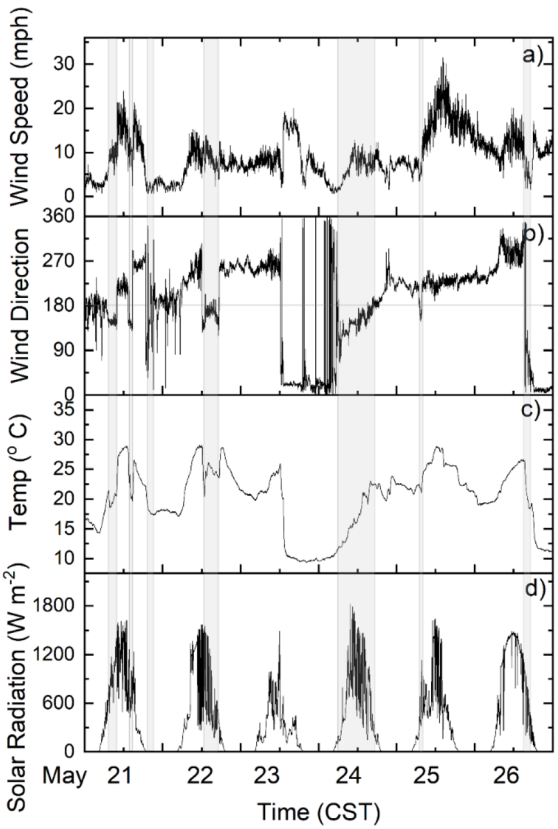


Fig. 2 Meteorological conditions as measured at the Wisconsin DNR Chiwaukee Prairie site from May 21–25, 2021: (a) wind speed (mph), (b) wind direction (degrees), (c) temperature (°C), (d) solar radiation (W $m^{-2}$). Lake breeze or onshore flow from SSE is highlighted.

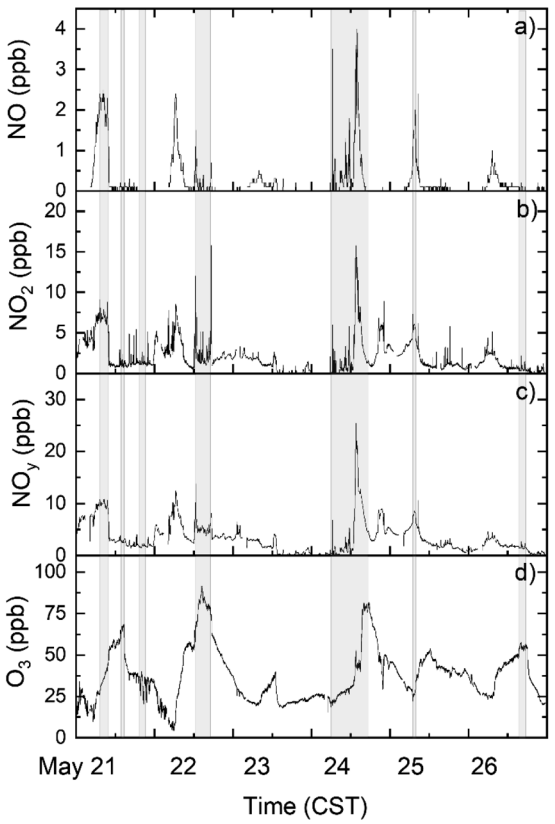


Fig. 3 Air quality ground station observations of (a) NO (ppb), (b) $NO_2$ (ppb), (c) $NO_y$ (ppb) and (d) $O_3$ (ppb) at Chiwaukee Prairie from May 21–26, 2021. Lake breeze or onshore flow from SSE is highlighted as grey bars.

decreased after lake breeze onset. The latest drop in temperature after lake breeze onset was the third lake breeze onset on May 21 where winds were slowly shifting to easterly (Fig. 2c). Wind speeds tended to be at a minimum near the lake breeze arrival, increasing after the wind direction change. Ozone generally increased within 2 hours of lake breeze onset (Fig. 3d), with such increases detected on five out of seven events. The days in which ozone did not increase after lake breeze onset were either very late (May 21-iii) or early in the day (May 24).

The contrast in ozone production and plume interception at this site can be seen in the differences in ozone concentrations in the mornings of May 22 and May 24, 2021. On May 22, ozone increases after the typical early morning minimum which can arise from $NO_x$ emissions titrating $O_3$. The lake breeze onset accompanies $O_3$ increases later in the day. On May 24, following northerly winds and frontal activity, ozone remains low until late in the afternoon, which can be attributed to interception of a Chicago plume later in the day with no residual $O_3$ in the lower atmosphere previously. The highest observed daily $O_3$ during days with lake breezes occurred during lake breezes (May 21, 22, 24 and 26) with the exception of the early morning May 25 lake breeze where NO and $NO_2$ concentrations were high (Fig. 3).

### 3.3 Evidence of lake breeze circulations aloft

Lake breeze circulation events can be identified by easterly winds near the surface in opposition to higher altitude synoptic winds as measured by Doppler lidar and UAS (Fig. 4 and 5). Two days with clear sustained lake breezes were on May 22 and May 24. On May 22, the RAAVEN was flying over land for all flights from an inland launch site (A) (see Fig. 1). A low temperature air mass was first observed *via* the M210 which launched closer to the shoreline (launch site B – Fig. 1) at about 18:30 UTC, and was observed by the RAAVEN operating a little further inland, where an easterly wind component (negative $u$ wind) was sustained by 19:00 UTC (see Fig. 4).

On May 22, 2021, a strong lake breeze accompanied with noted temperature inversions were detected late in the day. No easterly winds were observed for the first and most of the second RAAVEN flights (from around 14:00–18:00 UTC) (Fig. 4). However, breezes from over Lake Michigan began to be detected late in the second flight and throughout the entire third flight (from around 18:30–22:00 UTC). The vertical dimensions of the easterly wind component started around 100 m AGL at about 19:00 UTC and slowly reached around 300 m AGL by 20:00 UTC before decreasing back to around 200 m AGL at 22:00 UTC. The colder air indicative of a lake breeze was sustained over the sampling area from 18:30–22:00 UTC on May 22.[32] The time-period of low temperatures measured at the surface coincided with easterly winds observed by the RAAVEN (Fig. 4) and Doppler lidar.[32] The maximum extent of easterly winds extends up to ~300 m AGL at 21:00 UTC in RAAVEN data, which was similarly observed *via* Doppler lidar.[32]

May 24, 2021 was the day with the longest sustained lake breeze event detected during the campaign. RAAVEN flight data from over water and over land (flight pattern B) was segregated between over water and over land portions. An easterly wind component was observed for most of the sampling period (from 14:00–23:00 UTC) on May 24, observed at the lowest altitudes by the RAAVEN (Fig. 5b) and above 100 m AGL *via* lidar (Fig. 5a). By 17:30 UTC, easterly winds extended beyond 100 m AGL, gradually reaching 450 m AGL by 22:00 UTC. This shift was observed both by the Doppler lidar and RAAVEN (Fig. 5). The Doppler lidar showed some easterly flow at or below 100 m AGL from 14:00–16:00 UTC, whereas RAAVEN observations show continuity of easterly winds to the surface from 14:30–16:30 UTC. Combining the Doppler lidar observations with lower altitude measurements from the UAS provides complementary coverage of the atmosphere, with the UAS offering additional *in situ* temperature and humidity profiles to quantify marine layer thermodynamics. There is always a synoptic influence on marine air incursion at this location, wherein if the synoptic winds are too strong from the west, the lake breeze circulation will not occur (Laird *et al.*[36] 2001). It is clear from the wind fields aloft that the easterly component of $u$ winds on May 24 is not sustained to high altitudes and opposes a westerly flow aloft, signifying a layer of marine-influenced air more so than a sustained ground-level synoptic easterly flow.

### 3.4 Marine layer dimensions

The multiple daily UAS profiles enabled an investigation of how the marine boundary layer developed each day. Of particular interest was whether the marine air incursion over land differed from the marine air over water, and whether such differences persisted across days with and without lake breezes. In order to investigate the dimensions of the marine-influenced air, metrics for atmospheric inversion and stability of the atmosphere were calculated for atmospheric profiles to better constrain the depth of the marine-influenced layer.

There are several ways to identify different atmospheric layers from UAS observations. An inverted atmosphere, where temperatures are higher aloft, is negatively buoyant, which underlies the lack of cumulous cloud development over a marine-influenced air mass[17] (see Fig. S1–S6 in ESI†). One commonly used metric to determine atmospheric layers is the height of maximum buoyancy suppression, $h_{\max\text{-}N^2}$.[38] The $h_{\max\text{-}N^2}$ term represents the height at which buoyancy is most strongly suppressed (*i.e.*, the strongest part of the inversion). Buoyancy is derived from UAS temperature profiles, quantified as the square of the Brunt–Väisälä frequency, or buoyancy frequency ($N$):

$$N^2 = \frac{g}{\theta_v}\frac{\partial \theta_v}{\partial z} \quad (1)$$

where $g$ is acceleration due to gravity, $\theta_v$ is the absolute virtual potential temperature, and $z$ is altitude. This term provides a measure of the stability of fluid to displacement.

For an additional measure of the stability of the atmosphere, the UAS observations were used to calculate Richardson number. Here, because the data were collected as discrete points, we calculate bulk Richardson number ($R_B$):

$$R_B = \frac{g\Delta\theta_v\Delta z}{\theta_v\left[(\Delta u)^2 + (\Delta v)^2\right]} \quad (2)$$

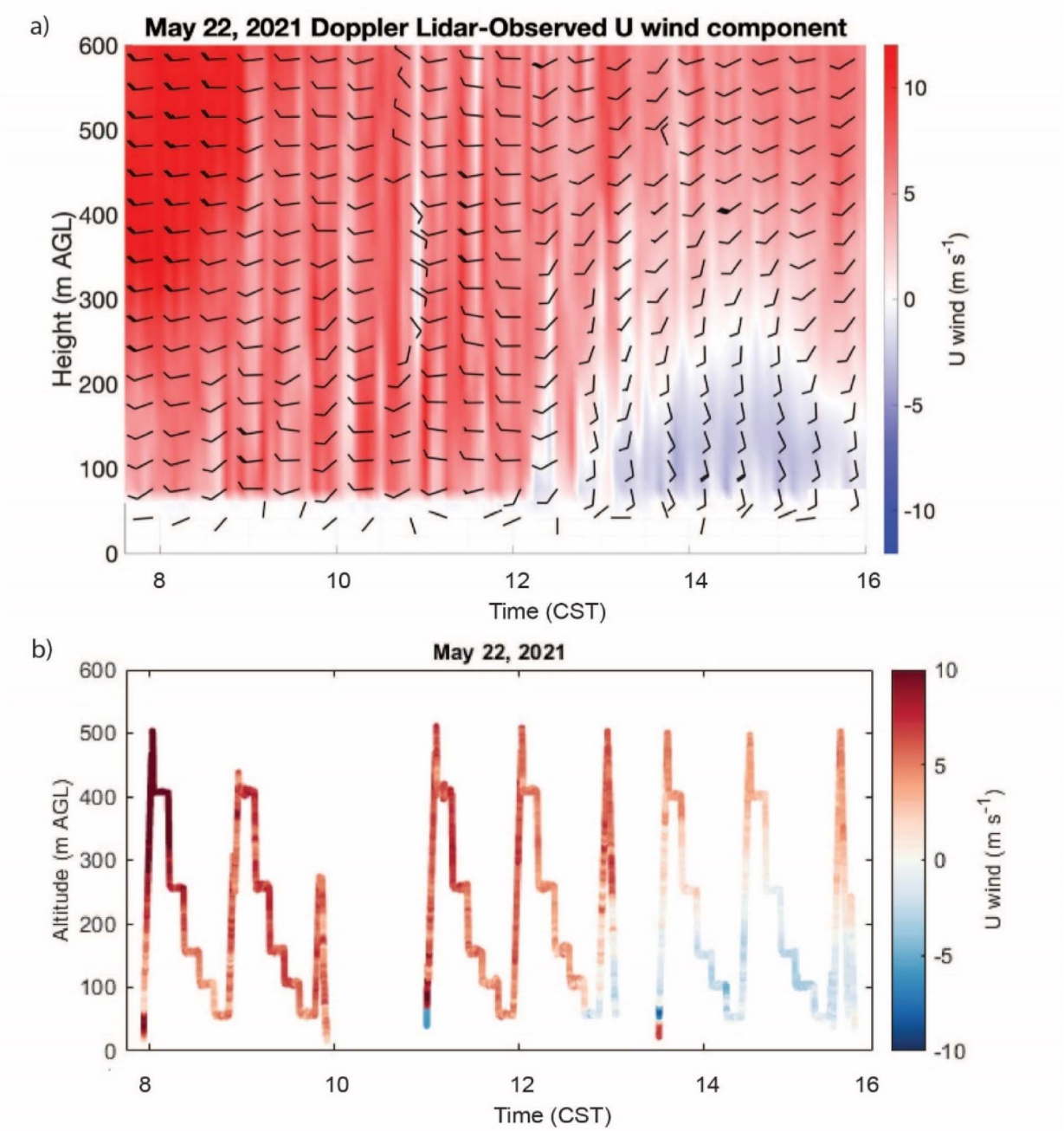


Fig. 4 Time–height cross section of the $u$ (zonal) wind component from (a) the Doppler-lidar-observed horizontal winds (in m $s^{-1}$), overlaid with horizontal wind barbs (in knots) plotted from 22 May 2021. Wind barbs are thinned by a factor of 5 in the time dimension and a factor of 2 in the height dimension to aid readability and (b) RAAVEN platform observations collected over land on May 22, 2021. In (a) is reprinted from Earth System Science Data with permission.[32]

where $u$ is the east-wind component of the wind, $v$ is the north–south component of the wind, and $\Delta$ represents the difference between discrete (here 1 m $\Delta z$) layers.[39] Empirical studies have found that atmospheric flows become turbulent when Richardson number falls below 0.25. While that threshold technically applies to the gradient Richardson number, it also approximates closely for $R_B$ calculated with thin $\Delta z$ layers.[39] In an inverted atmosphere, vertical mixing from buoyancy in the air parcels is suppressed, therefore turbulence is limited. Therefore, Richardson numbers above 0.25 demonstrate a less-turbulent vertical layer, which we also attribute to marine-influenced air.

For this analysis we focused on the two days during the campaign with the most developed lake breeze formations (May 22 and 24, 2021). The remaining days had more synoptically-driven conditions throughout the 0–500 m AGL measurement

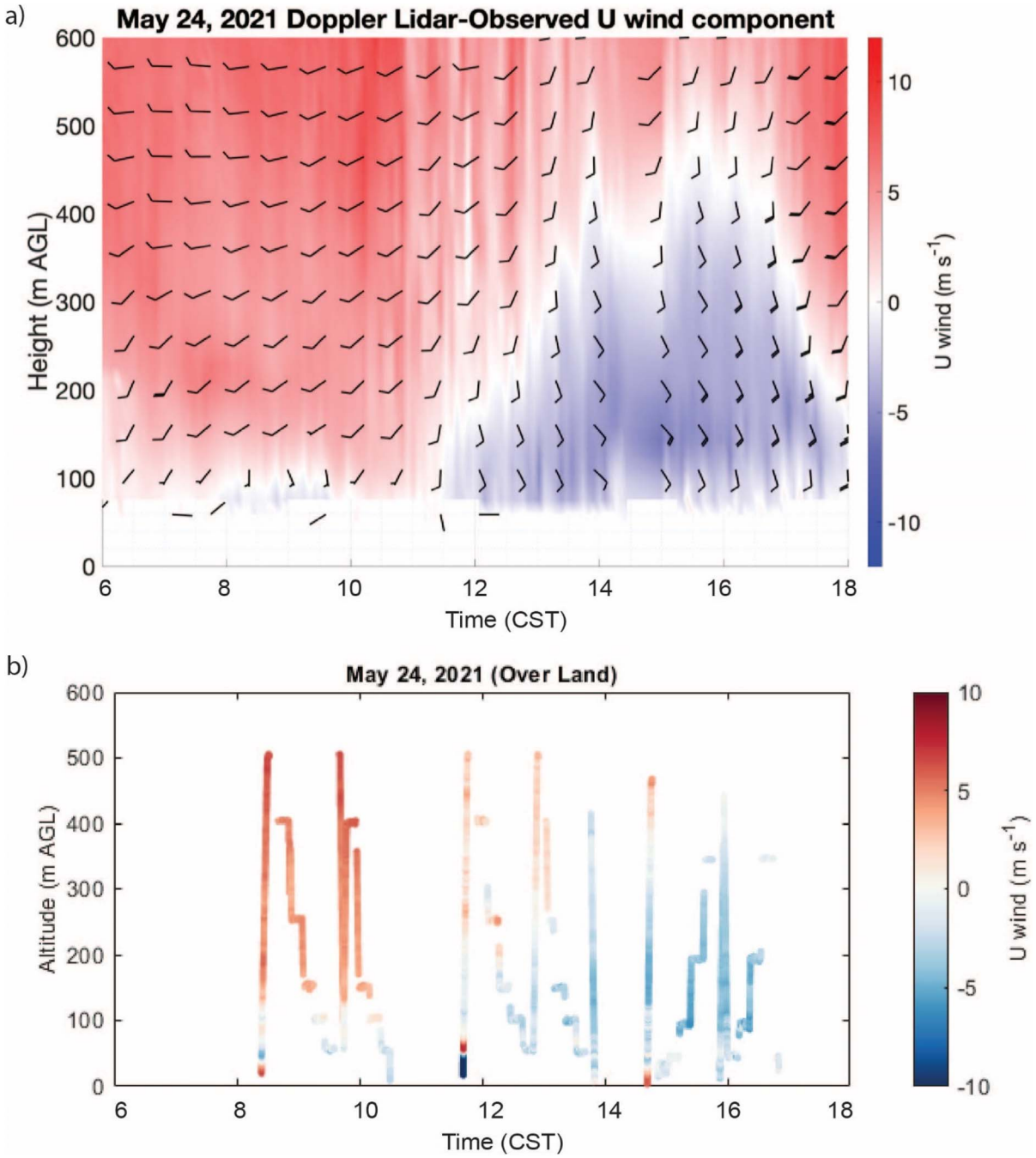


Fig. 5 Time–height cross section of the $u$ (zonal) wind component from (a) the Doppler-lidar-observed horizontal winds (in m $s^{-1}$), overlaid with horizontal wind barbs (in knots) plotted from 22 May 2021. Wind barbs are thinned by a factor of 5 in the time dimension and a factor of 2 in the height dimension to aid readability and (b) RAAVEN platform observations collected over land on May 24, 2021.

range, as indicated by constant $\theta$ lapse rates and relatively constant $U$ profiles. Additionally, on days other than May 22 and 24, $R_B$ indicated turbulent conditions throughout the lowest 500 m AGL, indicative of traditional, well-mixed, convective boundary layers. In order to capture the vertical profile of the atmosphere at a time when the atmospheric conditions were changing over time, the data from rapid descents or ascents were used to capture the vertical profile within a smaller time window. These ascents or descents were amid longer 2 hour flight times, so several of the ascents or descents did not extend to the surface because the aircraft was not landing.

The UAS profiles on May 22, 2021 were all collected over land. The morning and midday profiles showed a well-mixed atmosphere with westerly winds throughout the measurement range (Fig. 6). At 18:00 UTC the lake breeze initiated (Fig. 6b as seen in M210 temperature profile). Following this, the land $\theta$ profiles measured by both the RAAVEN and the M210 showed a surface inversion in the lowest 250 m AGL. Throughout the

 

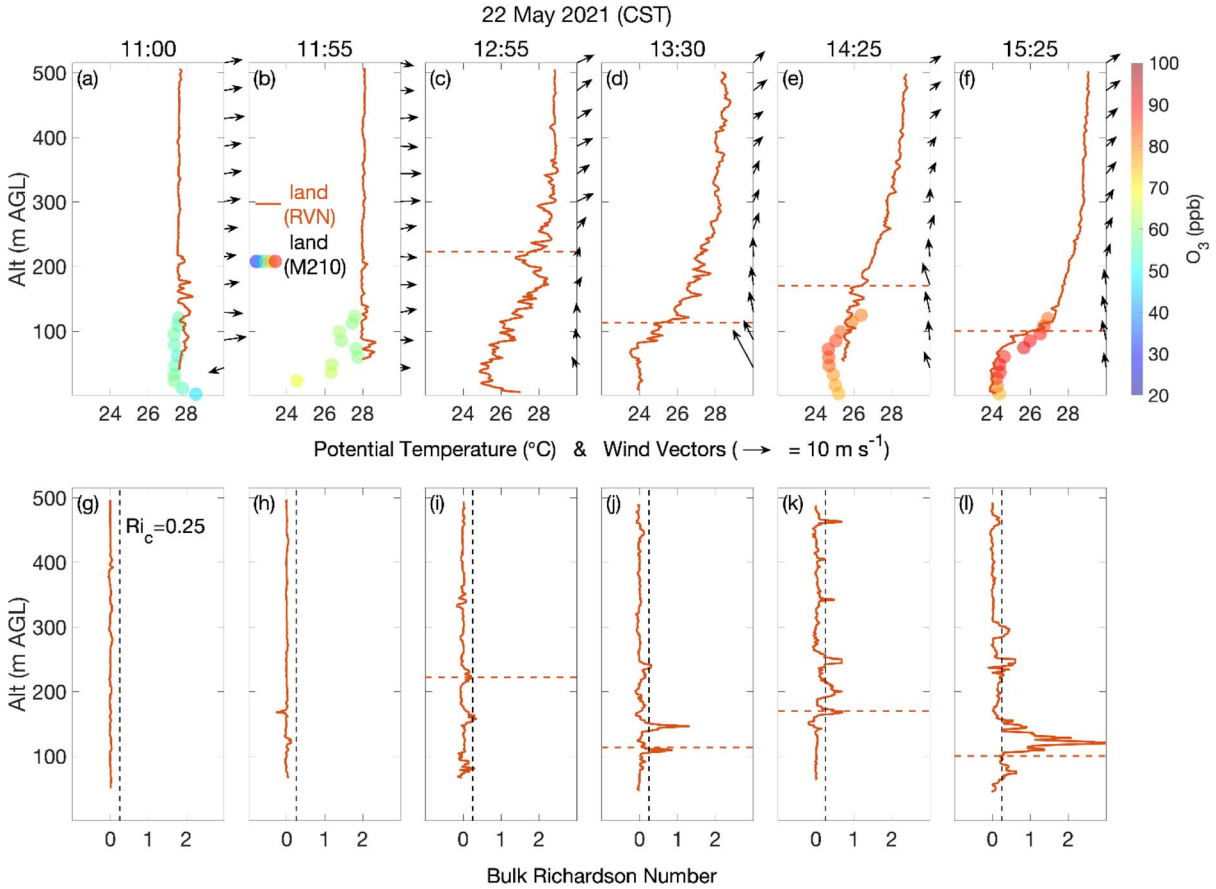


Fig. 6 (a–f) Show $\theta$ profiles for sets of profiling measurements spaced roughly one hour apart throughout May 22, 2021 (three morning profiles were omitted that had consistent behavior to the 17:00 and 17:55 UTC profiles). Orange lines represent RAAVEN profiles measured over land and M210 flights over land are depicted as $\theta$ profiles with $O_3$ colormap (ppb). Circles indicate $h_{\max\text{-}N^2}$. Wind vector profiles are shown at the righthand side of each panel. Arrow direction indicates azimuthal direction. Arrow length is relative to wind speed. (g–i) Show bulk Richardson number profiles, smoothed using a 20 m moving median.

inversion winds shifted to SSE, with westerly winds continuing aloft. The strongest portion of the inversion ($h_{\max\text{-}N^2}$) was located around 150 m AGL. Directly above $h_{\max\text{-}N^2}$ a stable layer was typically observed in the $R_B$ profiles, while below, conditions were typically well-mixed. The observations from May 22 are similar in nature to 2017 LMOS observations of lake breeze from Wagner, *et al.* where lake breeze days often featured well-mixed boundary layer conditions preceding lake breeze onset.[14]

May 24, 2021 followed a passage of a cold front on May 23. The presence of colder air beneath warmer air was also measured by RAAVEN and M210 over the sampling period on May 24 (Fig. 7) where the steepest changes in temperature lie at the lowest altitudes (<200 m AGL) throughout the day. Fig. 7 shows $\theta$, wind vector, and $R_B$ profiles observed on May 24, 2021. The morning $R_B$ profiles showed that the atmosphere was stable (*i.e.*, $R_B > 0.25$) throughout most of the measurement range, except for pockets of turbulence above 350 m AGL. Over both water and land, inversions extended from 50–350 m AGL, with $h_{\max\text{-}N^2}$ between 100–200 m AGL (Fig. 7a and b). Weak southerly winds below this height, transitioned to stronger westerly flow above. This suggests that $h_{\max\text{-}N^2}$ was a good measure of the marine layer height for this morning period. This is consistent with observations from 2017 LMOS, where lake breeze fronts were identified to extend to 100–200 m AGL with temperature inversion on the order of 8 K within 200 m.[14]

The midday profiles (Fig. 7c and d) showed a lowering of the strongest part of the inversion ($h_{\max\text{-}N^2}$ of roughly 100 m AGL) and consistent, well-mixed, convective conditions above 200 m AGL. During this period weak, southerly winds were observed through the entire measurement range. During the afternoon profiles (Fig. 7e–h), $h_{\max\text{-}N^2}$ remained near 100 m AGL. However, weaker inversions over both land and water stretched upwards to 400–500 m AGL. This led to increased atmospheric stability seen in the $R_B$ profiles (though notably, land profiles showed well-mixed conditions below $h_{\max\text{-}N^2}$, similar to May 22, 2021). It also corresponded with the transition to easterly flow from the surface to 400 m AGL. Because the easterly lake breeze extends up to 400 m AGL, it appears that the height of the inversion (not $h_{\max\text{-}N^2}$) is a better indicator of marine layer height during the afternoon period.

An observable difference between land and water profiles is apparent in this set of profiles from May 24, 2021. In the morning of May 24, the height of inversion, as indicated by $h_{\max\text{-}N^2}$, was decreasing from 190 m AGL at 8:30 CST (Fig. 7a) both over water

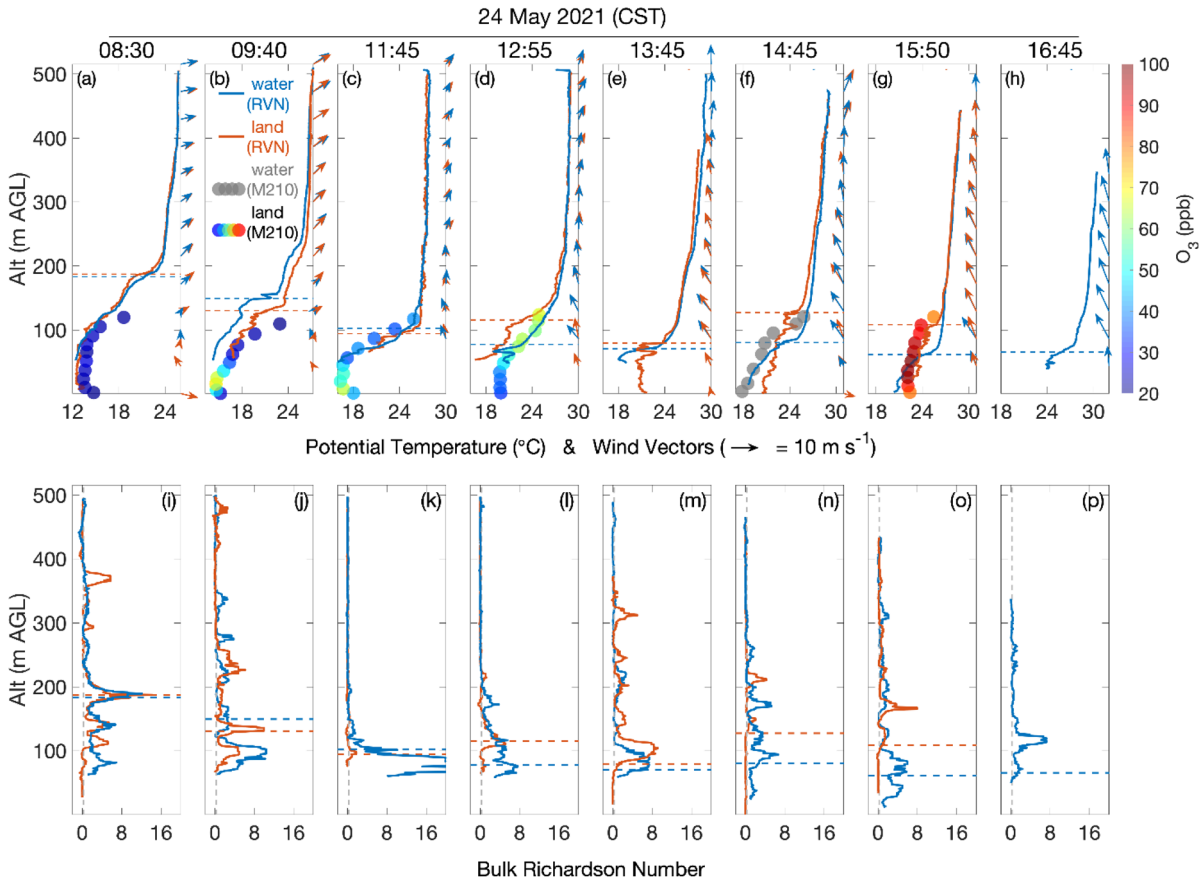


Fig. 7 (a–h) Show $\theta$ vertical profiles for sets of profiling measurements spaced roughly one hour apart throughout May 24, 2021. Orange and blue solid profiles represent RAAVEN profiles measured over land and water, respectively, while M210 flights over land are depicted as $\theta$ profiles with $O_3$ colormap (ppb) and M210 flight over water (grey). Dashed lines indicate $h_{max\text{-}N^2}$. Wind vector profiles are shown at the righthand side of each panel. Arrow direction indicates azimuthal direction. Arrow length is relative to wind speed. (i–p) Show bulk Richardson number vertical profiles, smoothed using a 20 m moving median.

and over land to 100 m AGL at 11:45 CST (Fig. 7c) both over water and over land. By the afternoon, higher $h_{max\text{-}N^2}$ was observed over land than over water (Fig. 7d through g). Below $h_{max\text{-}N^2}$, the land $R_B$ profiles showed well-mixed conditions; unlike the water profiles, which remained stable right down to the surface (Fig. 7f, g, n and o). Above $h_{max\text{-}N^2}$, the land $R_B$ profiles showed stable layers shifted slightly higher than corresponding water profiles (Fig. 7l–o). Two factors can increase $R_B$: low shear and/or potential temperature gradients. In the afternoon of May 24, the absence of potential temperature gradients above $h_{max\text{-}N^2}$ indicates that higher $R_B$ corresponded to slightly elevated low-level jets (where low shear increased $R_B$) over land compared to water profiles (Fig. 7l–o). Over land lidar also shows stronger winds at 100 m AGL on May 22 at 14:00 CST in the afternoon (Fig. 4) and between 150–300 m AGL on May 24 from 15:00–18:00 CST (Fig. 5). These jets could be indication of lake breeze circulation. Both the well-mixed surface conditions and the increasing height of the low-level jet over land, suggest the formation of an internal boundary layer (IBL) over the land of roughly 50–120 m AGL. A regime of conductive heating, friction from contact with the surface and turbulence slows down flow and increases mixing in the lowest 50–100 m AGL during the lake breeze circulation, and jets above those altitudes may show the overall directional circulation of the lake breeze driven at a higher altitude than directly at the surface. While $h_{max\text{-}N^2}$ during the afternoon period may be a residual of the morning inversion, over land it appears to maintain a role separating the IBL below from the marine layer above.

### 3.5 Relationship of $O_3$ and over land internal boundary layer

The M210 UAS platform was operated to observe ozone concentrations throughout the lowest parts of the atmosphere. In doing so, this system revealed a relationship between temperature inversions, the marine layer, and ozone concentrations. Fig. 6(a–f) and 7(a–h) display vertical profiles of ozone color mapped onto $\theta$ profiles collected by the M210 on May 22, 2021 and May 24, 2021. Morning observations of ozone tend to show higher ozone at low altitudes just above the surface (Fig. 6(a and b) and 7(b and c)) which may be from a continuous inversion at the site on May 24 following frontal activity on May 23, preventing mixing. At ~18:00 UTC a very shallow inversion is observed on May 22 (Fig. 6b) with a corresponding shallow area of high ozone from 10–40 m AGL. By mid-day to late afternoon, $O_3$ concentrations are at a maximum at altitudes at the top of the IBL (Fig. 6e, f and 7d) or at the $h_{max\text{-}N^2}$ over water (Fig. 7g).

These observations are consistent with the idea that ozone is readily mixed across the continental boundary layer, but that mixing between different stable layers is restricted. With the onset of a lake breeze featuring high ozone concentrations, and the subsequent development of a surface-coupled IBL, the ozone is trapped in an elevated layer, and being mixed into the surface internal boundary layer through entrainment at the layer interface. Losses of ozone are also present over land, with dry deposition and chemical titration from $NO_x$ emissions more abundant over land, which accounts for lower $O_3$ concentrations at the surface. The altitude of maximum ozone on May 24 (Fig. 7d and g) aligning with $h_{\max\text{-}N^2}$ over water hints at a mixing volume changing over a short distance from the shoreline, in which vertical profile of $O_3$ advects over land at $h_{\max\text{-}N^2}$ over water while broadening a vertical mixing volume over land. More observations comparing over water and over land ozone extent are required to test this hypothesis.

Ozone and other pollutants aloft have been shown to be associated with sea breezes and inversion at shoreline locations.[16,40] These observations are complementary to manned aircraft observations which indicated high ozone concentrations at very low altitudes (<100 m AGL) over water above Lake Michigan as a part of the 2017 LMOS.[5,12] Whereas, higher altitude features in ozone were observed by Gong, *et al.*[20] on the coast of Nova Scotia where the marine internal boundary layer was observed up to 100 m AGL and vertical profiles of ozone concentrations showed higher concentrations above the marine layer at altitudes 200–800 m AGL. Similarly, Sun *et al.*[21] studied lake breezes with a manned aircraft over Candle Lake in Saskatchewan which showed an internal boundary layer forming during daytime lake breezes showing amplified ozone at altitudes from 400–800 m AGL. The features described here agree better with a sea breeze from Galveston Bay which showed sea breeze features under 100 m AGL that grew throughout the day.[19] Wu, *et al.*[41] proposed that the vertical profiles of ozone at a site impacted by sea breezes demonstrate a lower altitude mixing layer and high ozone concentrations above an internal thermal boundary layer (at approximately 600–800 m AGL). What may differ between previous observations of sea breeze and ozone vertical profiles is the positioning of ozone precursor emissions and where within a stable atmosphere ozone is produced. These studies align with the observations from WiscoDISCO-21, although we have observed a very low altitude (<100 m AGL) internal boundary layer with high ozone regions within 120 m AGL, which could be specific to Lake Michigan, due to the direct injection of near-surface precursor emissions into the shallow Lake Michigan marine layer. However, future studies should fly UAS to higher altitudes to investigate the entire marine layer profile to better understand the ozone vertical structure within it.

Using relative humidity and temperature measurements from the RAAVEN UAS platform, we were able to estimate the height of the lifting condensation level (LCL)[42] (see Fig. S10†). The LCLs were calculated throughout all measurement days, before and after lake breeze fronts. They were calculated over water and over land. LCL heights did not differ over water *versus* over land. The LCL descended steadily through the week of measurements from roughly 1800 m AGL on May 21 to roughly 1200 m AGL on May 25, 2021. During the strongly stable conditions on 24 May, the LCL ranged from 100 to 1000 m AGL. On the final day of the campaign (May 26) the trend reversed and LCL increased to >2000 m. The extent of the LCL height well exceeds the observed phenomena of lake breeze circulation at lower altitudes. LCL estimates were close to those derived from nearest radiosondes in Green Bay and White Lake.

The analysis from the RAAVEN and Doppler lidar observations show inversion extending upwards to 400 m AGL when a lake breeze is present, with M210 and some low-altitude RAAVEN observations showing an internal boundary layer over land in the region of 40–100 m AGL, above which appears the strongest inversions and elevated concentrations of ozone. Further work should extend the observations of ozone above 120 m to test the hypothesis that during an inversion the ozone concentrations are high in regions of the highest inversion, specifically over water marine inversion.

## 4. Conclusions

The observations of lidar and two UAS each with some overlapping and complementary observations have allowed for a clearer representation of the vertical profile of the atmosphere in a shoreline environment, and how that vertical thermodynamic profile influences ozone pollutant distribution.

The presence of inversion is clear over water and air parcels over water show inversion to very low altitudes. When a marine air mass moves over land, an internal boundary layer develops which increases the height of maximum inversion. The positioning of the internal boundary layer and location of steep inversion appear to correlate with higher ozone concentrations, whereas lake breeze circulation of easterly components of wind extend up through shallower inversions to heights well above steep inversions in the late afternoon. Future efforts should explore the layering of ozone over water within the highly inverted atmosphere and the relationship between inversion and ozone to higher elevations.

## Author contributions

Joe Tirado, Akagaonye Torti, Brian Butterworth, and Aidan Voon were responsible for data analysis and manuscript writing. Ben Kies participated in data collection. Kevin Wangen contributed to data analysis. Joe Hupy contributed to data collection and manuscript writing. Gijs de Boer contributed to project management, data analysis and manuscript editing. R. Bradley Pierce contributed to field campaign planning, data collection and manuscript editing. Tim Wagner contributed to data collection, data analysis and manuscript editing. Patricia Cleary oversaw field campaign management, data acquisition, data analysis, manuscript writing and editing.

## Conflicts of interest

Gijs de Boer works as a consultant for Black Swift Technologies, who manufacture the multi-hole pressure probe used in the collection of the RAAVEN dataset.

## Acknowledgements

This work has been funded by the National Science Foundation Grant #AGS-1918850. We acknowledge financial assistance from the University of Wisconsin Blugold Differential Tuition program. We also acknowledge student support for J. Tirado from NSF Grant #1911284. Any opinions, findings, and conclusions or recommendations expressed in this material are those of the author(s) and do not necessarily reflect the views of the National Science Foundation. Gijs de Boer and Brian Butterworth were additionally supported by the NOAA Physical Sciences Laboratory.

## References

1 J. Fuhrer, *Ozone: Sci. Eng.*, 2002, **24**, 69–74.
2 T. M. Chen, J. Gokhale, S. Shofer and W. G. Kuschner, *Am. J. Med. Sci.*, 2007, **333**, 244–248.
3 W. F. McDonnell, *Environ. Toxicol. Pharmacol.*, 1996, **2**, 171–175.
4 J. E. Goodman, R. L. Prueitt, J. Chandalia and S. N. Sax, *J. Appl. Toxicol.*, 2014, **34**, 516–524.
5 P. A. Cleary, A. J. Dickens, M. McIlquham, M. Sanchez, K. Geib, C. Hedberg, J. Hupy, M. W. Watson, M. Fuoco, E. R. Olson, R. B. Pierce, C. Stanier, R. Long, L. Valin, S. Conley and M. Smith, *Atmos. Environ.*, 2022, **269**, 118834.
6 G. J. Lennartson and M. D. Schwartz, *Int. J. Climatol.*, 2002, **22**, 1347–1364.
7 W. A. Lyons and H. S. Cole, *J. Appl. Meteorol.*, 1976, **15**, 733–743.
8 W. A. Lyons and L. E. Olsson, *Mon. Weather Rev.*, 1973, **101**, 387–403.
9 C. S. Keen and W. A. Lyons, *J. Appl. Meteorol.*, 1978, **17**, 1843–1855.
10 T. S. Dye, P. T. Roberts and M. E. Korc, *J. Appl. Meteorol.*, 1995, **34**, 1877–1889.
11 T. Foley, E. A. Betterton, P. E. R. Jacko and J. Hillery, *Atmos. Environ.*, 2011, **45**, 3192–3202.
12 C. O. Stanier, R. B. Pierce, M. Abdi-Oskouei, Z. E. Adelman, J. Al-Saadi, H. D. Alwe, T. H. Bertram, G. R. Carmichael, M. B. Christiansen, P. A. Cleary, A. C. Czarnetzki, A. F. Dickens, M. A. Fuoco, D. D. Hughes, J. P. Hupy, S. J. Janz, L. M. Judd, D. Kenski, M. G. Kowalewski, R. W. Long, D. B. Millet, G. Novak, B. Roozitalab, S. L. Shaw, E. A. Stone, J. Szykman, L. Valin, M. Vermeuel, T. J. Wagner, A. R. Whitehill and D. J. Williams, *Bull. Am. Meteorol. Soc.*, 2021, **102**, E2207–E2225.
13 M. P. Vermeuel, G. A. Novak, H. D. Alwe, D. D. Hughes, R. Kaleel, A. F. Dickens, D. Kenski, A. C. Czarnetzki, E. A. Stone, C. O. Stanier, R. B. Pierce, D. B. Millet and T. H. Bertram, *J. Geophys. Res.: Atmos.*, 2019, **124**, 10989–11006.
14 T. J. Wagner, A. C. Czarnetzki, M. Christiansen, R. B. Pierce, C. O. Stanier, A. F. Dickens and E. W. Eloranta, *J. Atmos. Sci.*, 2022, **79**, 1005–1020.
15 K. L. Hayden, D. M. L. Sills, J. R. Brook, S. M. Li, P. A. Makar, M. Z. Markovic, P. Liu, K. G. Anlauf, J. M. O'Brien, Q. Li and R. McLaren, *Atmos. Chem. Phys.*, 2011, **11**, 10173–10192.
16 I. Levy, P. A. Makar, D. Sills, J. Zhang, K. L. Hayden, C. Mihele, J. Narayan, M. D. Moran, S. Sjostedt and J. Brook, *Atmos. Chem. Phys.*, 2010, **10**, 10895–10915.
17 D. M. L. Sills, J. R. Brook, I. Levy, P. A. Makar, J. Zhang and P. A. Taylor, *Atmos. Chem. Phys.*, 2011, **11**, 7955–7973.
18 J. Horel, E. Crosman, A. Jacques, B. Blaylock, S. Arens, A. Long, J. Sohl and R. Martin, *Atmos. Sci. Lett.*, 2016, **17**, 480–486.
19 R. M. Banta, C. J. Senff, J. Nielsen-Gammon, L. S. Darby, T. B. Ryerson, R. J. Alvarez, S. R. Sandberg, E. J. Williams and M. Trainer, *Bull. Am. Meteorol. Soc.*, 2005, **86**, 657–669.
20 W. M. Gong, R. E. Mickle, J. Bottenheim, F. Froude, S. Beauchamp and D. Waugh, *Atmos. Environ.*, 2000, **34**, 4139–4154.
21 J. L. Sun, R. Desjardins, L. Mahrt and I. MacPherson, *J. Geophys. Res.: Atmos.*, 1998, **103**, 25873–25885.
22 P. A. Cleary, N. Fuhrman, L. Schulz, J. Schafer, J. Fillingham, H. Bootsma, J. McQueen, Y. Tang, T. Langel, S. McKeen, E. J. Williams and S. S. Brown, *Atmos. Chem. Phys.*, 2015, **15**, 5109–5122.
23 R. T. McNider, A. Pour-Biazar, K. Doty, A. White, Y. L. Wu, M. M. Qin, Y. T. Hu, T. Odman, P. Cleary, E. Knipping, B. Dornblaser, P. Lee, C. Hain and S. McKeen, *J. Appl. Meteorol. Climatol.*, 2018, **57**, 2789–2816.
24 M. T. Odman, A. T. White, K. Doty, R. T. McNider, A. Pour-Biazar, M. M. Qin, Y. T. Hu, E. Knipping, Y. Wu and B. Dornblaser, *J. Appl. Meteorol. Climatol.*, 2019, **58**, 2421–2436.
25 M. M. Qin, H. F. Yu, Y. T. Hu, A. G. Russell, M. T. Odman, K. Doty, A. Pour-Biazar, R. T. McNider and E. Knipping, *Atmos. Environ.*, 2019, **202**, 167–179.
26 R. W. Arritt, *Bound.-Layer Meteorol.*, 1987, **40**, 101–125.
27 P. B. Chilson, T. M. Bell, K. A. Brewster, G. B. H. de Azevedo, F. H. Carr, K. Carson, W. Doyle, C. A. Fiebrich, B. R. Greene, J. L. Grimsley, S. T. Kanneganti, J. Martin, A. Moore, R. D. Palmer, E. A. Pillar-Little, J. L. Salazar-Cerreno, A. R. Segales, M. E. Weber, M. Yeary and K. K. Droegemeier, *Sensors*, 2019, **19**, 2720.
28 S. Illingworth, G. Allen, C. Percival, P. Hollingsworth, M. Gallagher, H. Ricketts, H. Hayes, P. Ladosz, D. Crawley and G. Roberts, *Atmos. Sci. Lett.*, 2014, **15**, 252–258.
29 D. E. Cook, P. A. Strong, S. A. Garrett and R. E. Marshall, *J. R. Soc. N. Z.*, 2013, **43**, 108–115.
30 P. Guimaras, J. H. Ye, C. Batista, R. Barbosa, I. Ribeiro, A. Medeiros, T. N. Zhao, W. C. Hwang, H. M. Hung, R. Souza and S. T. Martin, *Atmosphere*, 2020, **11**, 1371.
31 J. T. Sullivan, T. Berkoff, G. Gronoff, T. Knepp, M. Pippin, D. Allen, L. Twigg, R. Swap, M. Tzortziou, A. M. Thompson, R. M. Stauffer, G. M. Wolfe, J. Flynn, S. E. Pusede, L. M. Judd, W. Moore, B. D. Baker, J. Al-Saadi and T. J. McGee, *Bull. Am. Meteorol. Soc.*, 2019, **100**, 291–306.
32 P. A. Cleary, G. de Boer, J. P. Hupy, S. Borenstein, J. Hamilton, B. Kies, D. Lawrence, R. B. Pierce, J. Tirado, A. Voon and T. J. Wagner, *Earth Syst. Sci. Data*, 2022, **14**, 2129–2145.
33 P. A. Cleary, *J. Appl. Meteorol.*, 2021, 409–424.

34 J. Li, H. B. Chen, Z. Q. Li, P. C. Wang, X. H. Fan, W. Y. He and J. Q. Zhang, *Adv. Atmos. Sci.*, 2019, **36**, 1235–1250.
35 G. Pearson, F. Davies and C. Collier, *J. Atmos. Ocean. Technol.*, 2009, **26**, 240–250.
36 N. F. Laird, D. A. R. Kristovich, X. Z. Liang, R. W. Arritt and K. Labas, *J. Appl. Meteorol.*, 2001, **40**, 409–424.
37 G. J. Lennartson and M. D. Schwartz, *Clim. Res.*, 1999, **13**, 207–220.
38 B. B. Balsley, R. G. Frehlich, M. L. Jensen and Y. Meillier, *J. Atmos. Sci.*, 2006, **63**, 1291–1307.
39 R. B. Stull, *An Introduction to Boundary Layer Meteorology*, Springer, The Netherlands, 1988.
40 R. Lu and R. P. Turco, *J. Atmos. Sci.*, 1994, **51**, 2285–2308.
41 Y. L. Wu, C. H. Lin, C. H. Lai, H. C. Lai and C. Y. Young, *Terr. Atmospheric Ocean. Sci.*, 2010, **21**, 343–357.
42 D. M. Romps, *J. Atmos. Sci.*, 2017, **74**, 3891–3900.